Solar Energy Materials and Solar Cells 26 (1992) 117–136
North-Holland

Solar Energy Materials and Solar Cells

Studies on new chemically deposited photoconducting antimony trisulphide thin films

O. Savadogo [1] and K.C. Mandal

Département de Métallurgie et de Génie des Matériaux, École Polytechnique de Montréal, C.P. 6079, Succ. A, Montréal, Québec, Canada H3C 3A7

Received 3 August 1991; in revised form 15 October 1991

A new room temperature chemical deposition technique has been developed to deposit semiconducting antimony trisulphide thin films on conducting and ordinary glass substrates. The method is based on aqueous ammonia bath containing potassium antimonyl tartarate (PAT), triethanolamine (TEA) and thioacetamide (TAM). It has been found that the proper control of deposition bath compositions significantly influences the quality and the thickness of the Sb_2S_3 films. Moreover, addition of a small amount (10^{-5} M) of silicotungstic acid (STA) in the deposition bath enhanced the rate of deposition and improves significantly the photoactivity of the films. The deposited films were characterized by X-ray, SEM and neutronic activation analysis. The effect of the annealing and STA on the change of the optical bandgap (E_g) of the films was determined at 300 K. The influence of the STA on the resistivity, carrier concentrations and mobility of the films was determined by the resistivity and Hall effect measurements on the annealed samples. A very small ($\approx 5\%$) change in the electrical resistivity has been observed for the films in which STA is incorporated. X-ray photoelectron spectroscopic (XPS) studies were carried out to determine the surface and the bulk compositions of the films. The photoconductivity studies revealed that the deposited films were highly photoconducting in nature.

1. Introduction

Recently, there has been considerable interests for developing new polycrystalline thin film semiconductors using various techniques [1–5]. Among them, chemical deposition method has found out a special significance. Because this method is proved to be the least expensive, low temperature method and a non-pollutant one. Moreover, the quality of the films regarding the electrical and optical properties can be altered easily by incorporating suitable dopant materials in the chemical bath. So, no sophisticated technology such as photolithography, diffusion, ion implantation, etc., are required to achieve a material with desired properties. This method is also very suitable for making films of large area and of any configurations. Among the metal sulphides, antimony trisulphide finds special applications in target material for television cameras [6], microwave devices [7], switching devices [8] and various opto-electronic devices [9–11]. In all these cases,

[1] To whom correspondence should be addressed.

the films were prepared by the vacuum evaporation technique using powdered Sb_2S_3 as the starting material. This causes some departures in the stoichiometry of the deposited film which is mainly due to wide differences in the vapour pressures of the constituents at the deposition temperature. The present work describes for the first time a new chemical method for the deposition of Sb_2S_3 thin films and also the significant improvement of their properties when extremely high electrocatalytic material such as STA is used in the deposition bath. Composition variations of the chemical bath have been studied in detail to obtain the thickest possible films. The as-deposited and the annealed films were then characterized through X-ray, electrical and optical methods. The compositional analysis was performed by neutron activation analysis and the photoactivity of the films was evaluated by steady-state photoconductivity (PC) and by photoelectrochemical (PEC) measurements.

2. Experimental methods

2.1. Film deposition

Chemical deposition of Sb_2S_3 thin films was carried out by the reduction of Sb complexed with triethanolamine using thioacetamide as the reducing agent. For a typical film, the chemical bath composition was 25 ml of 0.1 M potassium antimonyl tartarate (BDH, AR), 5 ml of 7.4 M triethanolamine (BDH, AR), 3 ml of 17 M ammonia and various concentrations of STA in a 100 ml beaker. The mixed solution was stirred for 10 min to obtain a homogeneous solution. The solution was then diluted to 75 ml and the reduction was initiated by adding 25 ml of 0.1 M thioacetamide (BDH, AR) under a magnetic stirrer. Before use, the SnO_2-coated and the ordinary glass slides were cleaned ultrasonically in isopropyl alcohol and dried in a pure N_2 atmosphere. The cleaned substrates were then clamped vertically in the plating solution at 300 K. During the Sb_2S_3 film formation, the solution colour changed progressively from a faint to dark yellow and then finally to orange red, at which stage a thick deposition of Sb_2S_3 films were formed on the substrates. After about 96 h, the slides were removed and washed thoroughly by water and dried in air. In case of Sb_2S_3 films with STA, the same procedure was used with 5 ml of different concentrations of STA in the chemical bath.

2.2. Characterization

The structural characterization of the films were made using a Philips X-ray powder diffractometer using Ni-filtered Cu Kα radiation ($\lambda = 1.5405$ Å). The films from the substrates were scrapped for this purpose. The diffraction angles (2θ) corresponding to the X-ray peak intensities were identified and the calculated d values (lattice spacings) were compared with the standard d values form JCPDS [12] data file.

The surface morphologies were studied using a JEOL JXA-840 scanning electron microscope (SEM). The stoichiometry of the films was determined by neutron activation analysis, the details of the experimental assembly and the analysis have been reported elsewhere [13]. The thickness of each film have been estimated by weighing methods asssuming that the density of the film is the same as that of the bulk (4.61 g cm^{-3}). In few cases, the thickness of the films was measured by a sensitive stylus probe using sloan Dektak-II. In both the cases, the measured values of thicknesses were within an error of $\pm 5\%$.

Optical absorbance of the films was measured at 300 K in the transmission mode by using a Shimadzu UV/VIS spectrophotometer. A blank SnO_2 coated glass slide was placed in the reference beam and the spectra difference was recorded. The optical band gap was then determined by plotting $(\alpha h\nu)^{1/2}$ versus the photon energy $(h\nu)$.

Resistivity and Hall effect studies were conducted by using four-point probe van der Pauw technique. Ohmic contacts were provided by conducting silver paint, annealed at 150°C for 5 min in a N_2 atmosphere. For photoconductivity measurements, coplanar silver paint electrodes of 0.5 mm width and 20 mm length were applied on the surface of the films at a separation of 1 mm. A white light source (FIBER-LITE 180) of 300 W power whose intensities were calibrated by an Oriel Solar Simulator Radiometer (model 81020) was used. The light was incident from the film side. The applied bias was fixed at 20 V for all the cases. The current–voltage $(I–V)$ characteristics in the dark and under illumination were carried out using a KEPCO MSK 20-5 M DC variable voltage power supply, and the photocurrent was measured by a 614 Keithly electrometer. During illumination of the sample, the increase in temperature was not more than 1°C.

XPS investigations were carried out using a vacuum generator ESCALAB MK II ESCA/Auger spectrophotometer with MgKα source ($E = 1253.6$ eV). Emission energies of electrons from the Sb($3d_{5/2}$ and $3d_{3/2}$), Sb(4d), S(2p), O(1s) and C(1s) levels were examined and the intensities recorded directly. The nature of the surfaces in terms of the Sb : S ratio and the detection of the impurities introduced in the film from the deposition solution components or from the substrates were investigated before and after argon ion etching.

3. Results and discussion

3.1. Effect of chemical bath compositions

The formation of the Sb_2S_3 film is based on the slow release of Sb^{3+} and S^{2-} ions in an aqueous ammonia medium and then their subsequent condensation on the substrates. The following chemical equations for the formation of the films have been suggested:

$$SbO^+ + n\ TEA \longrightarrow SbO^+(TEA)_n \qquad (1)$$

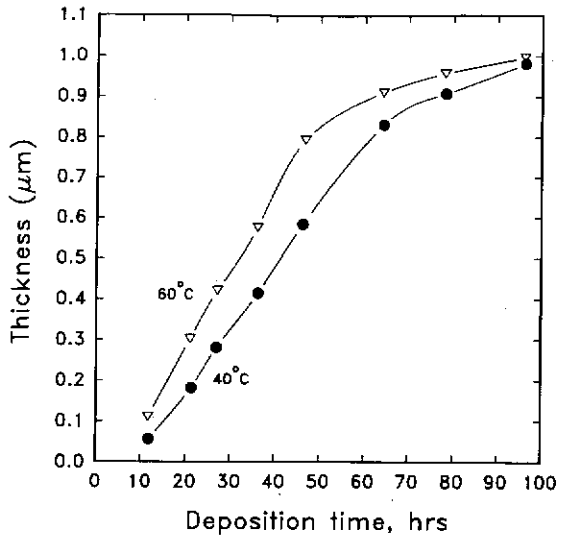

Fig. 1. Thickness variation of Sb_2S_3 film as a function of deposition time at (a) 40°C and (b) 60°C.

$$CH_3-\overset{\overset{S}{\|}}{C}-NH_2 \rightleftharpoons CH_3-\overset{\overset{SH}{|}}{C}=NH, \quad (2)$$

$$CH_3-\overset{\overset{SH}{|}}{C}=NH + OH^- \longrightarrow CH_3-\overset{\overset{OH}{|}}{C}=NH + SH^-, \quad (3)$$

$$2\,SbO^+(TEA)_n + 3\,SH^- \longrightarrow Sb_2S_3 + n\,TEA + OH^- + H_2O. \quad (4)$$

The tautomeric reactions (2) should proceed from left to right for the next step of reaction (3). It is clear from the above chemical reactions (1), (3) and (4), that the rate of deposition should be affected by the concentrations of PAT, TAM and NH_4OH. So, the chemical bath compositions were varied to optimize the conditions for deposition of the Sb_2S_3 films. The time dependence of the film thickness and the effect of chemical bath temperature were also studied.

From reactions (1) (3) and (4), it appears that the rate of deposition would increase with increasing concentrations of Sb^{3+}, SH^- and OH^- which are in agreement with the experimental results. Fig. 1 shows the time dependence of the film thickness. In the early stages of the film growth, the thickness increases at a very fast rate. Then the rate decreases resulting in a terminal thickness. At 40°C, the rate of film growth is slow (1.89 Å/min) and terminal thickness of 0.97 μm attained after 96 h. However, at 60°C the growth rate is higher (2.8 Å/min) and a terminal thickness of ≈ 1.0 μm is attained after a period of 96 h.

The effect of various concentrations of PAT and TAM on the film thicknesses measured at 313 K and 333 K are represented in figs. 2 and 3. It is clear from the figures that the rate of film deposition increases regularly up to the concentration of 0.25 M PAT. The growth rate is also higher at higher temperature (333 K). As

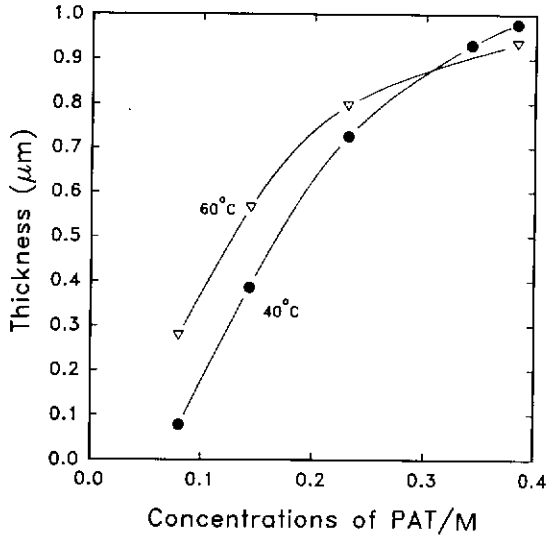

Fig. 2. Effect of the PAT concentration on the growth of the Sb_2S_3 films, (a) at 40°C and (b) at 60°C.

in case of CdS [14], this may be explained on the basis of higher rate of release of Sb^{3+} and S^{2-} ions in the solution. Moreover, at higher temperature the kinetic energy of the released ions are higher causing increased interaction between them and the subsequent condensation at the volume nucleation centres of the substrates [1].

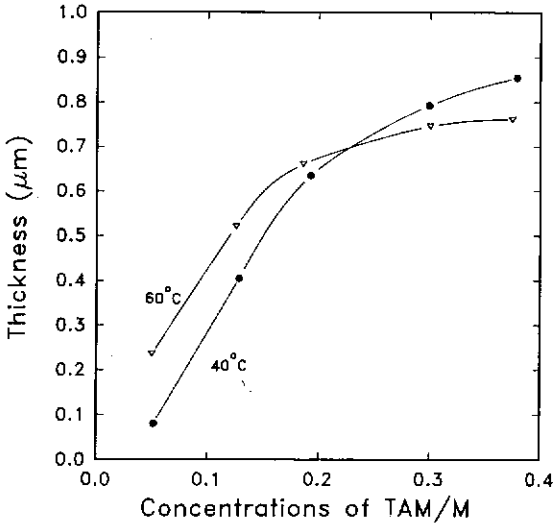

Fig. 3. Effect of the TAM concentration on the growth of the Sb_2S_3 films, (a) at 40°C and (b) at 60°C.

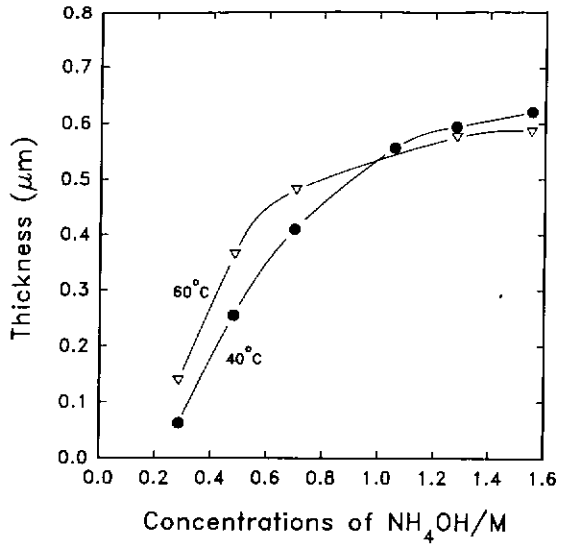

Fig. 4. Effect of the NH_4OH concentration on the growth of the Sb_2S_3 films, (a) at 40°C and (b) at 60°C.

The dependence on the film thickness of Sb_2S_3 and the concentration of NH_4OH is shown in fig. 4. This figure shows that the deposited film thickness gradually increases with the increase of OH^- concentration and saturates from 1.4 M concentration. Further increase of OH^- concentration drastically increases the bulk precipitation of Sb_2S_3 rather than the enhanced film thickness. It is interesting to indicate that Sb_2S_3 films deposited with STA(Si) are more thicker and more photosensitive (described later) than that of Sb_2S_3 films deposited without it. This effect of the STA on the deposited film thickness and the improvement of the optoelectronic properties is under present investigations.

3.2. X-ray characterization

The X-ray diffraction pattern of the as-deposited Sb_2S_3 film powder scrapped off the SnO_2 coated glass substrates is shown in fig. 5a. The appearence of the broad X-ray spectrum suggested an amorphous structure. The same trend has been observed when the film is deposited with STA. After annealing at 300°C for 1 h in a N_2 atmosphere, the powdered samples showed well defined crystallographic planes (fig. 5b) and these were identified in the recordings [12]; the structural features are consistent with an orthorhombic cell with lattice constants $a_0 = 11.269$, $b_0 = 11.299$ and $c_0 = 3.824$ Å. No other peaks due to impurities or other phases were observed within the sensitivity of the instruments. The (211), (221) and (310) peaks were found to have the highest intensities and in agreement with the literature [15].

Fig. 5. X-ray di
deposited film w

From the
annealed at 3
to WO_3 (Fig.
From the X-r
triclinic phase

3.3. Scanning

Sb_2S_3 films
glass and stain
6a and 6b sh
substrates bef
surface withou
clearly demons
talline growth.
substantial gra
films deposited
showed a more
on this aspect a
The effect o
gated. Ordinary
this purpose. T
regular texture,

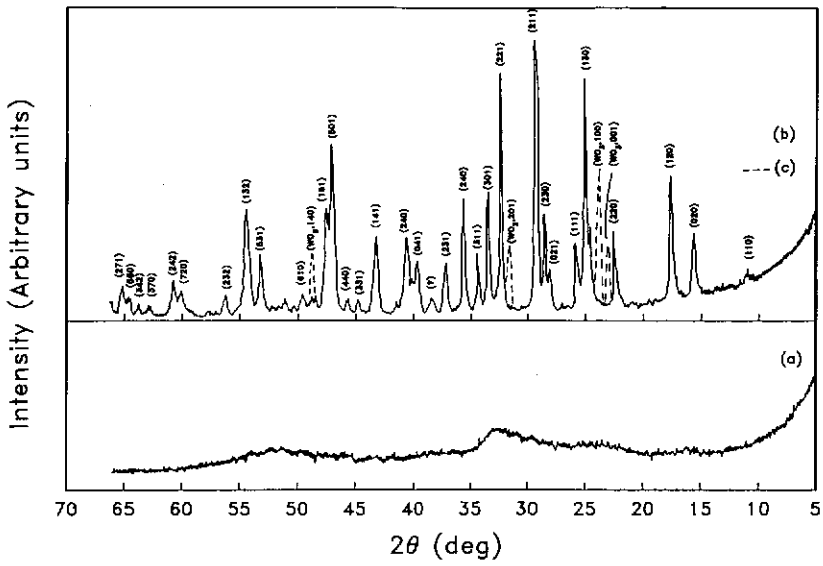

Fig. 5. X-ray diffractograph of an Sb_2S_3 film scraped off the SnO_2-coated glass substrates: (a) as deposited film with and without 10^{-5} STA; (b) with annealing at 300°C for 1 h in a N_2 atmosphere (without STA) and (c) same as (b) but with 10^{-5} M STA.

From the X-ray examination on the Sb_2S_3 films prepared with STA and annealed at 300°C, in addition to Sb_2S_3 lines there also arises the intense peak due to WO_3 (Fig. 5c) which has been incorporated in the Sb_2S_3 film during deposition. From the X-ray peak positions the structural features of WO_3 was identified as the triclinic phase with the lattice constant $a_0 = 7.28$, $b_0 = 7.56$ and $c_0 = 3.836$ Å.

3.3. Scanning electron microscopy studies

Sb_2S_3 films deposited on various substrates such as ordinary glass, SnO_2-coated glass and stainless steel have been used for studying the surface morphology. Figs. 6a and 6b shows the SEM micrographs of Sb_2S_3 films on SnO_2-coated glass substrates before and after annealing. In these micrographs, a homogeneous, surface without cracks or holes were observed. The as-deposited film (fig. 6a) clearly demonstrates an uneven surface morphology devoid of any granular crystalline growth. Annealing the films at 300°C in a N_2 ambient for 1 h shows a substantial granular growth with a significant increase of grain size. Moreover the films deposited with 10^{-5} M STA and annealed with the same conditions as above showed a more pronounced grain growth on the substrates. The different studies on this aspect are kept open as an avenue for future investigations.

The effect of changing the substrate on film deposition has also been investigated. Ordinary glass slides and stainless steel (SS) substrates have been used for this purpose. The as-deposited film (not shown) in both cases do not reflect any regular texture, which is a plain smooth surface. Fig. 6c shows the deposited Sb_2S_3

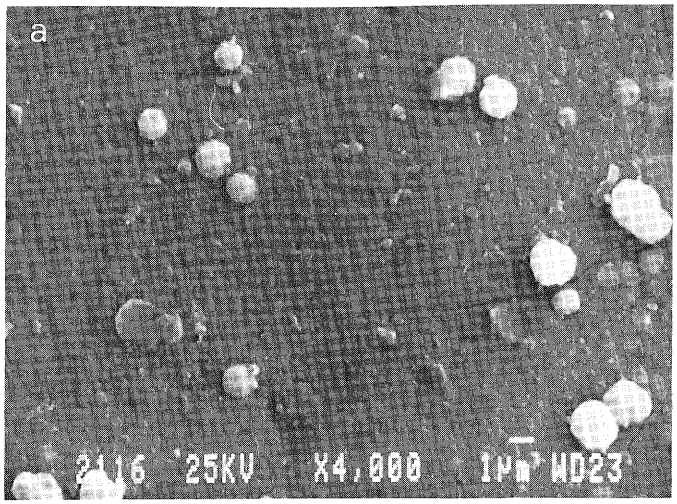
a
2116 25KV X4,000 1μm WD23

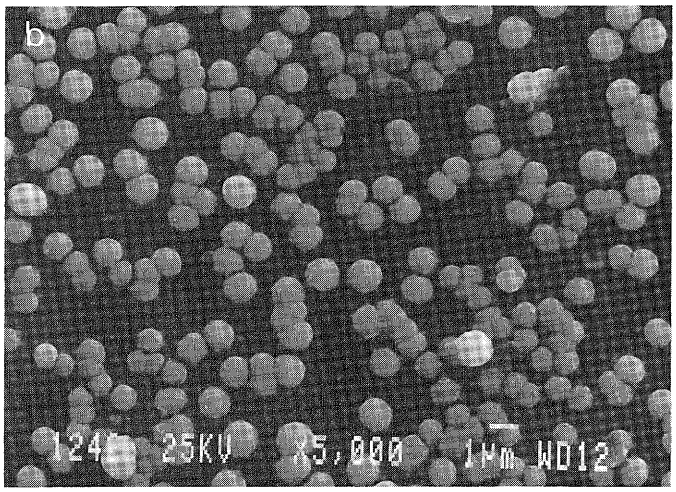
b
1245 25KV X5,000 1μm WD12

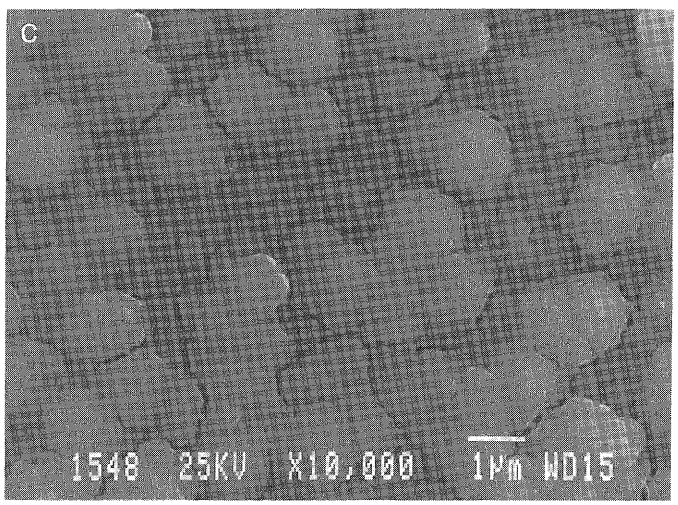
c
1548 25KV X10,000 1μm WD15

Table 1
Comparison of grain sizes and electrical properties of the different films (for experimental conditions, see text)

Sample substrate	Grain sizes (μm)	Resistivity ρ (Ω cm)	Carrier concentrations N_d (cm^{-3})	Mobility μ_n (cm^2/Vs)
Sb_2S_3 film, SnO_2 coated glass				
as deposited	0.12 ± 0.02	3.8×10^8		
annealed	0.82 ± 0.01	5.3×10^6	1.2×10^{12}	9.8
Sb_2S_3 film, STA, SnO_2 coated glass				
as deposited	0.25 ± 0.02	4.2×10^8	–	–
annealed	1.02 ± 0.2	5.0×10^6	2.4×10^{12}	9.2
Sb_2S_3 film, ordinary glass side				
as deposited	0.06 ± 0.02	4.6×10^8	–	–
annealed	0.08 ± 0.02	4.2×10^8	–	–
Sb_2S_3 film, stainless steel				
as deposited	0.11 ± 0.02	6.4×10^8	–	–
annealed	0.64 ± 0.1	4.8×10^8	–	–

film on the glass and annealed at 300°C in a N_2 atmosphere for 1 h. This picture clearly demonstrates that a second phase of large grain material is growing on the otherwise featureless substrates.

The grain sizes were evaluated from the micrographs by Cottrell's method [16]; this method relates the number of intercepts of grain boundary per unit lengths P_L and is given by $P_L = (n/2\pi r)M$, where n is the total number of intercepts and M is the magnification. Using P_L, the grain size, L, was determined, since

$$L = 1/(P_L - 1).$$

The values of grain sizes are given in table 1. The as-deposited films have very small grains. A significant increase in the grain size occurs when the films are deposited with STA and subsequently annealed at 300°C, 1 h in a N_2 atmosphere. The values of grain sizes (table 1) show that the annealed films deposited with STA on SnO_2-coated glass substrates have essentially much larger grains than that on the ordinary glass substrates, since the Sb_2S_3 films were deposited on SnO_2-coated glass, which is comparatively more textured than the ordinary glass slide.

Fig. 6. Scanning electron microscope pictures of Sb_2S_3 films deposited on SnO_2-coated glass substrate: (a) as-deposited; (b) annealed at 300°C for 1 h in a N_2 atmosphere. (c) same as (b) but 10^{-5} STA incorporated in the chemical deposition bath.

Table 2
Composition analysis for the various Sb_2S_3 films

Film and substrate used	Element	Content (at%)	
		As-deposited	Annealed at 300°C
Sb_2S_3, ordinary glass side	Sb	31.2	34.7
	S	68.8	65.3
Sb_2S_3, Stainless steel substrate	Sb	33.5	35.8
	S	66.5	64.2
Sb_2S_3, SnO_2 coated glass substrate	Sb	34.3	36.2
	S	65.7	63.8
Sb_2S_3 STA, SnO_2 coated glass substrate	Sb	35.1	38.6
	S	64.9	61.4

3.4. Stoichiometry determination: neutron activation analysis

A comparison of the atomic percents of Sb and S present in the different films are given in table 2. In order to optimize measurement conditons, the powdered sample (scrapped off the substrates) of about 1 g was irradiated at least three times with the flux of 10^{12} neutrons/cm^2 s and counted four times with a liquid nitrogen cooled Ge gamma ray detector. The compositional data represented in table 2 showed that a near-stoichiometric film was obtained when the film was deposited with 10^{-5} M STA into SnO_2-coated glass substrates and thermally annealed in a N_2 atmosphere at 300°C for 1 h. It is to be noted here that W, C, O and Sn impurities appeared in XPS analysis (shown later) could not be identified in this analysis.

3.5. Optical absorption studies

The optical absorption spectra of the as-deposited and annealed films are recorded at 300 K and are shown in figs. 7a and b. The values of the optical absorption coefficient (α) were not corrected for the transmittance and the reflectance of the film surface. The optical data were analysed from the following classical expression for near-edge optical absorption in semiconductors

$$\alpha = \frac{k(h\nu - E_g)^{n/2}}{h\nu},$$

where k is a constant, E_g is the semiconductor bandgap and n is a constant equal to 1 for direct gap and 4 for an indirect gap compound. Since the plots of $(\alpha h\nu)^{1/2}$ versus $h\nu$ are linear, the indirect nature of the optical transition in Sb_2S_3 is confirmed. Extrapolation of these curves to zero absorption coefficient gives the optical energy gap (E_g) which is 1.86 eV for unannealed sample and 1.74 eV for the annealed sample. The decrease in E_g after heat treatment of as-deposited Sb_2S_3 film is in agreement with the behaviour shown previously for CdS and CdSe

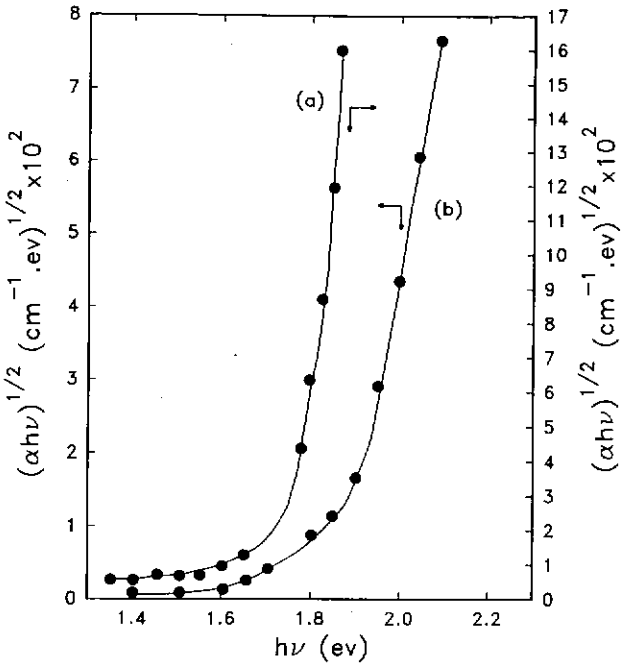

Fig. 7. Variation of $(\alpha h\nu)^{1/2}$ versus $(h\nu)$ for a typical film on SnO_2-coated glass substrate: (a) Sb_2S_3 film prepared with 10^{-5} M STA and an nealed at 300°C in a N_2 atmosphere for 1 h, (b) same as (a) but without STA and (c) as deposited film without STA.

thin films [17,18]. This behaviour is explained by an increase in effective grain size on annealing. The latter value of E_g agrees closely with the value of 1.77 eV for polycrystalline Sb_2S_3 films [19].

3.6. Resistivity and Hall effect studies

Thermoelectric power measurements were conducted which showed that both the as-deposited and the annealed films with and without STA are n-type in nature. Four-point probe determination of resistivity on the as-deposited Sb_2S_3 film on SnO_2 coated glass substrates gave a value of about 3.8×10^8 Ω cm. After the thermal treatment (300°C for 1 h in a N_2 atmosphere), the resistivity decreased to 5.3×10^6 Ω cm. The decrease in resistivity after thermal annealing may be due to the formation of sulphur vacancies and is also confirmed by compositional analysis. The Hall coefficient (R_H) was experimentally determined on the annealed samples at room temperature and from the relation $\mu_n = |R_H\sigma|$ where μ_n is the Hall mobility and σ the conductivity, the electron mobility was found to be 9.8 cm^2/Vs. The carrier concentration was determined from the relation $n = 1/qR_H$ and was found to be 1.2×10^{12} cm^{-3}. The resistivity and Hall effect measurements on the as-deposited and the annealed films with STA showed the

same trend except that the annealed films had σ and μ_n approximately 6% lower than the values reported without STA.

The temperature dependence of electrical resistivity was determined between 200 and 335 K for the annealed specimens with (10^{-5} M) and without STA. The activation energies (E_a) were determined from the slopes of log σ versus $1/T$ variation. The E_a values were found to be 0.53 eV and 0.56 eV respectively for the specimens without and with STA. These values agree very well with the results obtained by Montrimas et al. [10]. It is also interesting to note that the activation energy of sample prepared without STA is the same than that of Sb_2S_3 fabricated with STA.

3.7. XPS measurements

The different Sb_2S_3 film surfaces were evaluated and characterized for better understanding of their surface properties by XPS (X-ray photoelectron spectroscopy). In the present work, XPS has been used to investigate the surface compositions and the detection of impurities introduced in the films from the deposition solution components or from the substrates. Fig. 8a shows an XPS survey spectrum with the peak assignments of the annealed (300°C in a N_2 atmosphere for 1 h) Sb_2S_3 films. Trace amount of O, Sn (may be from the substrate), N and C were detected in the film. Argon ion etching for few minutes removed substantially the O, N and C contaminants but the small peak height for the presence of Sn remained unchanged while etching providing thereby the effect from the substrates. Fig. 8b shows the survey spectrum of Sb_2S_3 film deposited with 10^{-5} M STA and annealed in the same conditions as above. It is observed that, other than O, Sn, N and C in the film, there arises a sharp peak spectrum for W.

Fig. 9 represented the high resolution analyses of the binding energy peaks of the Sb $3d_{3/2}$ and $3d_{5/2}$ energy levels on the as-prepared annealed surfaces (A). Notably, there arises a shoulder at about 531.6 eV corresponding to the Sb_2O_3 energy levels. After in situ mild argon-ion etching for 30 s, the higher energy shoulder disappeared completely and the lower energy peak height was considerably enhanced (B). It is shown later that the chemically shifted higher energy shoulder is due to Sb^{3+}, present on the surface in the form of a thin layer of Sb_2O_3, while the lower energy intense peaks are due to the Sb in Sb_2S_3. The emission spectra (fig. 10) for the Sb(4d) peaks at binding energy 36.4 eV being characteristic of the Sb in Sb_2S_3 with all the fine structures due to the d^{10} final states.

Examination of the S spectra (fig. 11) on the as-deposited and annealed surfaces failed to reveal any chemically shifted lines. In the S(LMM) Auger spectra there was no evidence of any shift to lower kinetic energy. Hence it may be inferred that there is no evidence of the formation of any S-related compounds, other than Sb_2S_3 on the surface. Comparing the spectra before and after argon etching showed an increase (by factor of 13) of the intensity of the Sb line on Sb_2S_3 films showing the increased concentration of Sb in the bulk. Examination of the O(1s)

Counts ($\times 10^5$)

Counts ($\times 10^5$)

Fig. 8. XPS surve

level was also
weak before ar
the Sb_2S_3 film
The reporte
Sb_2S_3 are 529.
values determi
shoulder) was
Ar-ion etching.
shoulder) displa

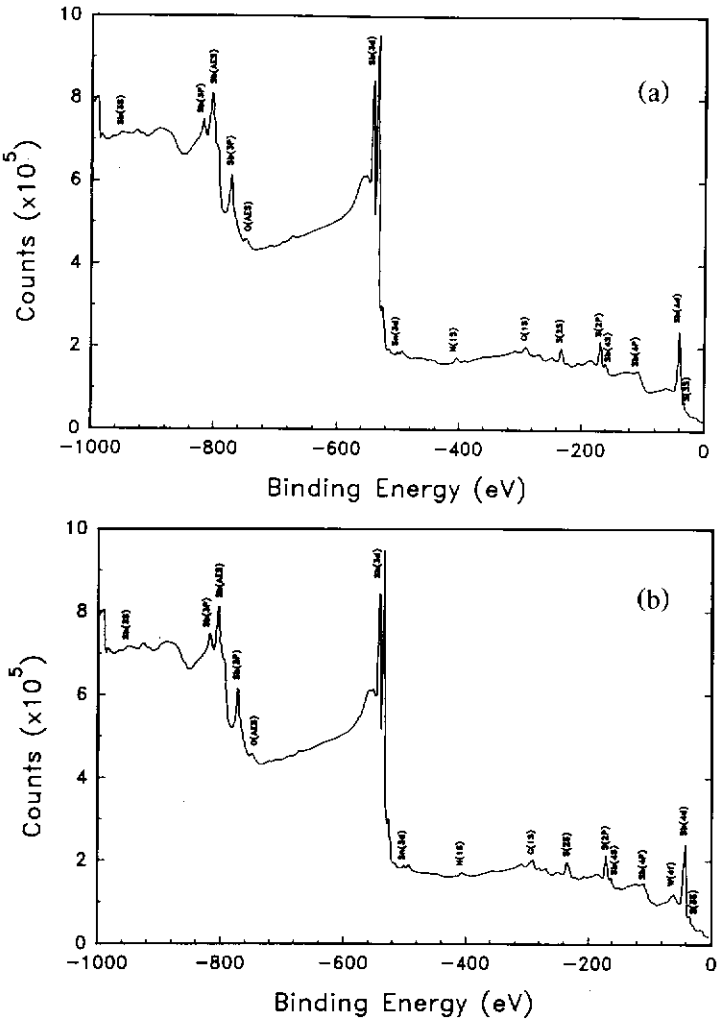

Fig. 8. XPS survey scan for the annealed Sb_2S_3 film surface. (a) Sample fabricated without STA; (b) sample fabricated with STA.

level was also carried out and was found that the line corresponding to O(1s) was weak before argon-ion etching, after etching there is no evidence of any oxides at the Sb_2S_3 film surface.

The reported binding energies [20] for Sb($3d_{5/2}$ and $3d_{3/2}$) and Sb(4d) levels in Sb_2S_3 are 529.3, 538.7 and 36.4 eV respectively which agree very well with the values determined from figs. 9 and 10. In fig. 9 the additional energy levels (i.e. as shoulder) was found at 531.6 eV on the annealed as-prepared surfaces before Ar-ion etching. But after argon etching there is no trace of it. This energy levels (as shoulder) displays a chemical shift of 1.0 eV representing an Sb^{3+} in the Sb_2O_3

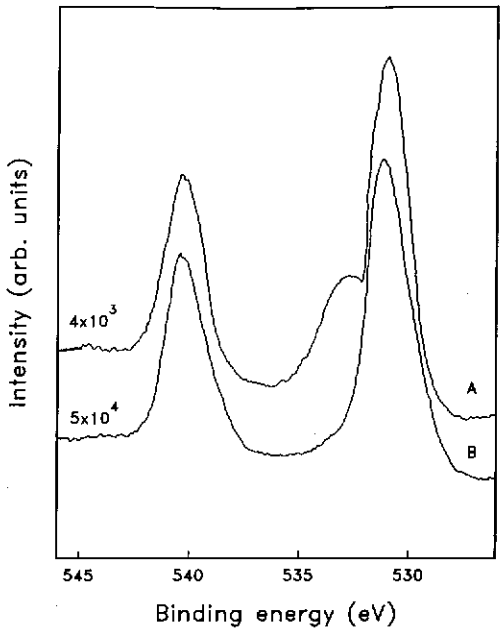

Fig. 9. Photoemission spectra of Sb(3d) levels; (A) as-prepared annealed surface, (B) after 30 s argon-ion etching.

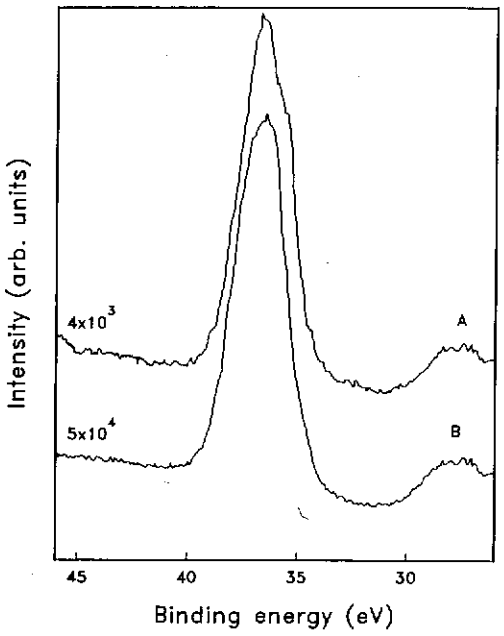

Fig. 10. Photoemission spectra of Sb(4d) levels; (A) as-prepared annealed surface, (B) after 2 min argon-ion etching.

Fig. 11. Photoem

state. High re
incorporated S
W($4f_{5/2}$ and 4
that after 1 mi
as with before
and $4f_{5/2}$) hav
which also con
film.

The surface
peak intensitie
results are give
Sb while argon
fact that the XI
tion leading to
annealing N_2 at

3.8. Photocondu

Fig. 13 repr
illumination. Th
increase up to t
within the grai
photoconductive

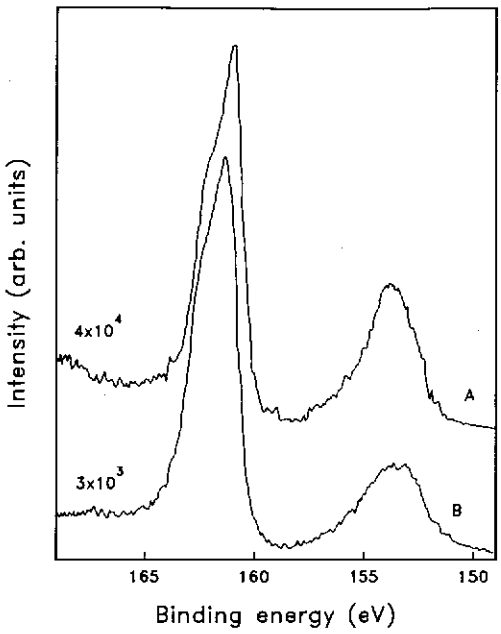

Fig. 11. Photoemission spectra of S(2p) levels; (A) as-prepared annealed Sb_2S_3 surface, (B) after 2 min argon-ion etching.

state. High resolution analysis of the XPS spectra for the annealed and STA incorporated Sb_2S_3 films with and without Ar etching is represented in fig. 12. The W($4f_{5/2}$ and $4f_{7/2}$) energy levels are at 31.3 and 33.7 eV respectively. It is observed that after 1 min of argon sputtering of the film, the peak height remains the same as with before argon etching. Moreover homogeneous distribution of the W($4f_{7/2}$ and $4f_{5/2}$) have been confirmed when the sputter cycling is continued for 15 min which also confirmed that incorporated W from the surface to the depth of the film.

The surface compositions in terms of the Sb:S ratio was determined from the peak intensities taking into account the photoionization cross sections. These results are given in table 3 and show that the unetched surfaces reveal depletion of Sb while argon-ion etched (3 min) show reasonably stoichiometric. In view of the fact that the XPS samples prior to argon-ion etching, were stored before examination leading to ambient oxidation or the oxidised layer may come from the annealing N_2 atmosphere which has a little contamination with oxygen (4–6 ppm).

3.8. Photoconductivity studies

Fig. 13 represents the current–voltage characteristics in the dark, and on illumination. The difference between dark current and photocurrent is seen to increase up to the voltage range of study of 20 V. The role of barrier resistances within the grain boundaries may be responsible for the difference [21]. The photoconductive decay curves for various Sb_2S_3 films are represented in fig. 14

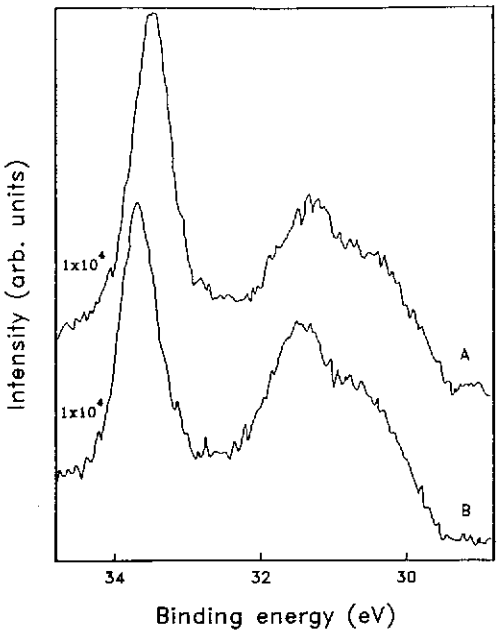

Fig. 12. Photoemission spectra of W (4f) levels; (A) as-prepared annealed surface, (B) after 1 min argon-ion etching.

and the light to dark current ratios in tables 4a and 4b). From fig. 14 and tables 4 it is clear that the decay curves for the film which is exposed in air for longer period of time is much more slower and also the I_{pc}/I_{dc} decreased continously with the exposure periods in air. The dark current also shows to increase significantly. This behaviour may be explained on the basis of atmospheric oxygen diffusion to the grain boundaries in Sb_2S_3 films and the creation of the opposite type of charge carriers in n-type Sb_2S_3. Oxygen is known to act as an acceptor impurities. Similar

Table 3
Composition of Sb_2S_3 film surfaces as determined by XPS

Film conditions and substrate used	Etching conditions		Ratio of atomic species Sb:S
Sb_2S_3 film on SnO_2 coated glass	As-deposited	without Ar etching	1:1.97
		after Ar etching	1:1.92
	Annealed	without Ar etching	1:1.68
		after Ar etching	1:1.76
Sb_2S_3 film STA [10^{-5} M] on SnO_2-coated glass side	As deposited	without Ar etching	1:1.85
		after Ar etching	1:1.71
	Annealed	without Ar etching	1:1.82
		after Ar etching	1:1.58

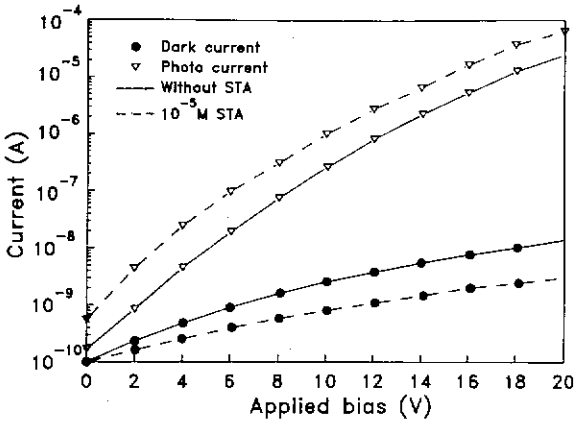

Fig. 13. Current (I)–voltage (V) characteristics of Sb_2S_3 with and without STA; (●) in the dark, (△) under illumination.

behaviour has also been found in CdS and CdSe films. The diffusion of oxygen into the sulphur vacancies and the decrease of photosensitivity as in case of the present studies were observed earlier in CdS films and in single crystals [21,22]. The details of a feasible mechanism which could account for this effect will be published in our future paper. Finally, the effect of STA incorporation in the Sb_2S_3 films have been examined by photoconductivity studies. The considerable improvement of the photosensitivity is represented in fig. 14, curves b′, c′ and d′, for the rise and decay of the photoconductivity curves.

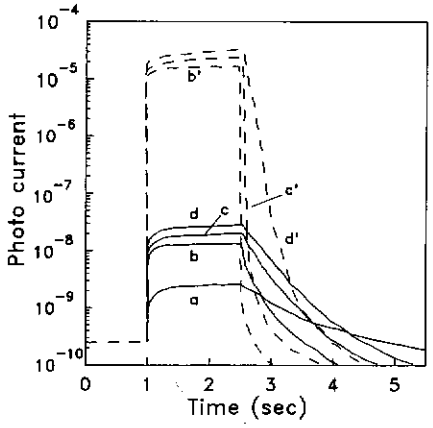

Fig. 14. Photoconductive rise and decay curves for the Sb_2S_3 films at various conditions: (a) as-deposited Sb_2S_3 film, unannealed, (b, b′) annealed at 300°C for 1 h in a N_2 atmosphere, (c, c′) same as (b, b′) but storage in air at 30°C for 5 h, (d, d′) same as (b, b′) but storage in air at 30°C for 24 h. (Excitation voltage = 20 V, photoexcitation intensity = 100 mW/cm^2; photocurrent in A). The light is switched on at $t = 1$ s and switched off at $t = 2.5$ s.

Table 4a
Dark and photocurrent response of chemically deposited Sb_2S_3 film with various concentrations of silicotungstic acid, applied voltage 20 V, annealed sample (300°C for 1 h in a N_2 atmosphere)

Surface conditions	Concentrations of silicotungstic acid (STA)								
	Without STA			10^{-6} M STA			10^{-5} M STA		
	I_{dc} ($\times 10^{-9}$ A)	I_{pc} ($\times 10^{-6}$ A)	I_{pc}/I_{dc} ($\times 10^{3}$)	I_{dc} ($\times 10^{-9}$ A)	I_{pc} ($\times 10^{-6}$ A)	I_{pc}/I_{dc} ($\times 10^{3}$)	I_{dc} ($\times 10^{-9}$ A)	I_{pc} ($\times 10^{-6}$ A)	I_{pc}/I_{dc} ($\times 10^{4}$)
Freshly annealed	21.2	45.6	2.15	18.6	48.3	2.6	5.2	64.8	1.2
After 5 h of storage in air at 30°C	31.6	21.4	0.7	25.4	41.4	1.6	7.3	59.7	0.8
After 10 h of storage in air at 30°C	43.4	9.8	0.2	29.3	36.2	1.2	12.4	54.5	0.4
After 25 h of storage in air at 30°C	56.2	5.8	0.1	37.0	31.5	0.8	17.8	49.2	0.3
After 48 h of storage in air at 30°C	66.4	2.2	0.03	44.8	21.8	0.5	23.5	41.0	0.2

Table 4b
Same as table 4a with other concentrations of silicotungstic acid

Surface conditions	Concentrations of silicotungstic acid (STA)								
	10^{-4} M STA			10^{-3} M STA			10^{-2} M STA		
	I_{dc} ($\times 10^{-9}$ A)	I_{pc} ($\times 10^{-6}$ A)	I_{pc}/I_{dc} ($\times 10^{3}$)	I_{dc} ($\times 10^{-9}$ A)	I_{pc} ($\times 10^{-6}$ A)	I_{pc}/I_{dc} ($\times 10^{3}$)	I_{dc} ($\times 10^{-9}$ A)	I_{pc} ($\times 10^{-6}$ A)	I_{pc}/I_{dc} ($\times 10^{3}$)
Freshly annealed	9.4	59.1	6.3	13.2	5.27	3.9	15.8	49.9	3.2
After 5 h of storage in air at 30°C	14.6	54.0	3.7	18.5	47.3	2.5	22.8	44.7	1.9
After 10 h of storage in air at 30°C	21.2	48.3	2.3	23.1	41.5	1.8	28.6	35.8	1.2
After 25 h of storage in air at 30°C	27.6	39.2	1.4	28.4	34.9	1.2	36.5	29.7	0.8
After 48 h of storage in air at 30°C	35.5	31.0	0.9	37.7	21.8	0.6	48.3	19.2	0.4

4. Conclusions

From the results reported here, it can be concluded that: (a) A new chemical method has been developed to deposit photoactive semiconductor grade Sb_2S_3 thin films. (b) The significant improvement of the film properties have been obtained by introducing a small concentration of STA (10^{-5}) in the deposition bath. (c) The as-deposited films are amorphous in nature but annealing treatment (300°C for 1 h in a N_2 atmosphere) leads to more stoichiometric and polycrystalline films. (d) The optical bandgap of the as-deposited film changed from 1.86 to 1.74 eV after annealing. (e) The films are n-type with resistivity, carrier concentration and mobility 5.3×10^6 Ω cm, 1.2×10^{12} cm^{-3} and 9.8 $cm^2/V s$ respectively. (f) WO_3 was detected on the films deposited with STA. (g) The activation energy was found to be 0.53 eV and 0.56 eV for the films deposited without and with STA respectively.

References

[1] R.C. Kainthla, D.K. Pandya and K.L. Chopra, J. Electrochem. Soc. 127 (1980) 277.
[2] D.M. Schleich, H.S. Chang, Y.I. Barberio and K.J. Hanson, J. Electrochem. Soc. 136 (1989) 3274.
[3] J.R. Lince, J. Mater. Res. 5 (1990) 218.
[4] K.C. Mandal and O. Savadogo, J. Mater. Chem. 1 (1991) 301.
[5] K. Saiki, K. Ueno, T. Shimada and A. Koma, J. Crystal Growth 95 (1989) 603.
[6] D. Cope, U.S. Patent No. 2,875,359 (1959).
[7] J. Grigas, J. Meshkauskas and A. Orliukas, Phys. Status Solidi (a) 37 (1976) K39.
[8] M.S. Ablova, A.A. Andreev, T.T. Dedegkaev, B.T. Melekh, A.B. Peutsov, N.S. Shendel and L.N. Shumilova, Soviet Phys. Semicond. 10 (1976) 629.
[9] M.J. Chockalingam, K. Nagarajo Rao, N. Ranjarajan and C.V. Suryanarayana, J. Phys, D 3 (1970) 1641.
[10] E. Montrimas and A. Pazera, Thin Solid Films 34 (1976) 65.
[11] J. George and M.K. Radhakrishna, Solid State Commun. 33 (1980) 987.
[12] Powder Diffraction File, JCPDS (1987).
[13] O. Savadogo and K.C. Mandal, Mater. Chem. Phys., in press.
[14] A. Mondal and P. Pramanik, J. Solid State Chem. 47 (1983) 81.
[15] Swanson et al., Natl. Bur. Stand. (U.S.) Circ. 539 (1955) 56.
[16] A. Cottrell, in: An Introduction to Metallurgy (Arnold, London, 1975) p. 173.
[17] H. Weller, H.M. Schmidt, U. Koch, A. Fotjick, S. Baral, A. Henglein, W. Kunath, K. Weiss and E. Dieman, Chem. Phys. Lett. 124 (1986) 557.
[18] G. Hodes, A.A. Yaron, F. Decker and P. Motosuke, Phys. Rev. B 36 (1987) 4216.
[19] A. Viehbeck and N. Hackerman, Proc. Symp. Photoelectrochemistry: Fundamental Processes and Measurement Techniques. The Electrochem. Soc. (1987) p. 478.
[20] W.E. Morgan, J.S. Wojeiech and J.R. Van Wazer, Inorg. Chem. 12 (1973) 953.
[21] C. Wu and R.H. Bube, J. Appl. Phys. 45 (1974) 648.
[22] J.W. Orton, B.J. Goldsmith, J.A. Chapman and M.J. Powell, J. Appl. Phys. 53 (1982) 1602.